Accepted Manuscript

Please cite this article as: V.B. Oliveira, C.M. Rangel, A.M.F.R. Pinto, One-dimensional and non-isothermal model for a passive DMFC, *Journal of Power Sources* (2008), doi:10.1016/j.jpowsour.2011.01.094

ONE-DIMENSIONAL AND NON-ISOTHERMAL MODEL FOR A PASSIVE DMFC

V.B. Oliveira*****, C.M. Rangel [o] and A.M.F.R. Pinto*****[#]

*Centro de Estudos de Fenómenos de Transporte, Departamento de Eng. Química,

Faculdade de Engenharia da Universidade do Porto

Rua Dr. Roberto Frias, 4200 – 465 Porto – Portugal

[o] Laboratório Nacional de Energia e Geologia,

Paço do Lumiar, 22,1649-038 – Portugal

[#] corresponding author Email: apinto@fe.up.pt

Abstract

Passive direct methanol fuel cells (DMFCs) are promising energy sources for portable electronic devices. Different from DMFCs with active fuel feeding systems, passive DMFCs with nearly stagnant fuel and air tend to bear comparatively less power densities. A steady state, one-dimensional, multi-component and thermal model is described and applied to simulate the operation of a passive direct methanol fuel cell. The model takes into consideration the thermal and mass transfer effects, along with the electrochemical reactions occurring in the passive DMFC. The model can be used to predict the methanol, oxygen and water concentration profiles in the anode, cathode and membrane as well as to estimate the methanol and water crossover and the temperature profile across the cell. Polarization curves are numerically simulated and successfully compared with experiments for different methanol feed concentrations. The model predicts with accuracy the influence of the methanol feed concentration on the cell performance and the correct trends of the current density and methanol feed concentration, on methanol and water crossover. The model is rapidly implemented and

1

is therefore suitable for inclusion in real-time system level DMFC calculations. Due to its simplicity the model can be used to help seek for possibilities of optimizing the cell performance of a passive DMFC by studying impacts from variations of the design parameters such as membrane thickness, catalyst loading, diffusion layers type and thicknesses.

Nomenclature

a	specific surface area of the anode, cm^{-1}
A_a	active area, cm^2
A_1	total area without the holes, cm^2
A_{holes}	total area of the holes, cm^2
C	concentration, mol/cm^3
C_2	concentration at the AAP/ACP interface, mol/cm^3
C_3	concentration at the ACP/AD interface, mol/cm^3
C_4	concentration at the AD/AC interface, mol/cm^3
C_5	concentration at the AC/membrane interface, mol/cm^3
C_6	concentration at the membrane/CC interface, mol/cm^3
C_7	concentration at the CC/CD interface, mol/cm^3
C_8	concentration at the CD/CCP interface, mol/cm^3
$C_{O_2,ref}$	reference concentration of oxygen, mol/cm^3
Cp	specific heat capacity, J/(molK)
$\partial E / \partial T$	rate of change of electromotive force, V/K
D	diffusion coefficient, cm^2/s
D^{eff}	effective diffusion coefficient, cm^2/s
E_{Cell}	thermodynamic equilibrium potential, V
F	Faraday´s constant, 96500 C/mol
G	Gibbs free energy, J/mol
g	gravitational acceleration, cm^2/s
H	enthalpy of reaction, J/mol
h_{mass}	mass transfer coefficient, cm/s
h_{heat}	heat transfer coefficient, W/(cm^{2}K)
I_{Cell}	cell current density, A/cm^2
I_{CH_3OH}	leakage current density due to methanol crossover, A/cm^2
$I_{0,ref}^{CH_3OH}$	exchange current density of methanol, A/cm^2
$I_{0,ref}^{O_2}$	exchange current density of oxygen, A/cm^2
j_A	volumetric current density, A/cm^3
k	constant in the rate expression (Eq. (27))
K_{2-8}	partition coefficients
K	thermal conductivity, W/(cmK)
L	length of the active area, cm
n_d	electro-osmotic drag coefficient of water

2

N	molar flux, mol/(cm^{2}s)
P_{air}	pressure of air in cathode, atm
Q^{AC}	heat generated in AC, W/cm^2
Q^{CC}	heat generated in CC, W/cm^2
Q	heat transfer, W
R	gas constant, 8.314 J/(molK)
R_{Cell}	internal resistance of the fuel cell, cm^2/S
R_{cond}	conduction resistance, K/W
R_{conv}	convection resistance, K/W
R_{total}	total thermal resistance, K/W
T	temperature, K
U_{CH_3OH}	thermodynamic equilibrium potential of methanol oxidation, V
U_{O_2}	thermodynamic equilibrium potential of oxygen oxidation, V
V_{Cell}	cell voltage, V
x_{CH_3OH}	mole fraction of methanol, mol/mol
x	coordinate direction normal to the anode, cm

Greek

Δ	variation
α	net water transport coefficient
α_A	anodic transfer coefficient
α_C	cathodic transfer coefficient
β	coefficient of volume expansion, 1/K
δ	thickness, cm
ε	porosity
η	overpotential, V
κ	ionic conductivity of the membrane, S/cm
λ	constant in the rate expression (Eq. (27)), mol/cm^3
μ	dynamic viscosity, g/(cms)
ν	kinematic viscosity, cm^2/s
ρ	density, g/cm^3
υ_{O_2}	stoichiometric coefficients of oxygen in the cathode reaction
υ_{H_2O}	stoichiometric coefficients of water in the cathode reaction
υ_{cross,O_2}	stoichiometric coefficients of oxygen in the undesired cathode reaction
υ_{cross,H_2O}	stoichiometric coefficients of water in the undesired cathode reaction
ξ_{CH_3OH}	electro-osmotic drag coefficient of methanol

Subscripts

A	anode
air	air
C	cathode
CH_3OH	methanol
i	species i
j	species j
H_2O	water

O_2	oxygen

Superscripts

0	feed conditions
AAP	anode acrylic plate
ACP	anode copper plate
AC	anode catalyst layer
AD	anode diffusion layer
CAP	cathode acrylic plate
CC	cathode catalyst layer
CCP	cathode copper plate
CD	cathode diffusion plate
l	plate l
M	membrane
t	plate t

Keywords – Passive Direct Methanol Fuel Cell, Modelling, Heat and mass transfer, Methanol crossover, Water Crossover

1. Introduction

Conventional batteries are becoming inadequate for the increasing power requirements of portable electronic devices such as mobile phones, PDA's, laptops and multimedia equipment. Direct methanol fuel cells (DMFCs) are promising candidates as portable power sources because they do not require any fuel processing resulting in a simpler design and operation, higher reliability and operate at low temperatures. DMFCs offer high energy densities, longer runtime, instant recharging and lower weight than conventional batteries. The most significant obstacle for DMFC development is methanol crossover, since methanol diffuses through the membrane generating heat but no power. This problem can be limited if the cell operates with low methanol concentration on the anode. However, this significantly reduces the system energy density since water will produce no power and will take up a large volume in the fuel reservoir. Due to the concentration gradient between the anode and cathode, water

4

crosses through the membrane. The presence of a large amount of water floods the cathode and reduces cell performance.

There are two types of fuel and oxidant supply in a DMFC: an active and a passive one. Active systems use extra components such as a pump or blower, a fan for cooling, reactant and product control, which allows the operation of a DMFC at favourable conditions with respect to temperature, pressure, concentration and flow rate. This type of system supply is more complex, has greater costs and lower system energy densities. More recently, the passive DMFCs have been proposed and investigated [1-17]. Passive systems use natural capillary forces, diffusion, convection (air breathing) and evaporation to achieve all processes without any additional power consumption. Therefore, the fuel cell system becomes much simpler and more compact being more suitable for portable power sources. The passive DMFCs have much lower power density due to the inability to handle the excess water produced on the cathode and crossed from the anode and to the excess of heat lost from the fuel cell to the ambient air. Therefore, the key issues in the portable DMFC system is the thermal and water management [5,12,14-17].

Performance of a passive DMFC relies on a vast number of parameters, including the methanol feed concentration, efficiencies of methanol and oxygen transport within the different layers, the release rate of gaseous carbon dioxide and its effect on methanol transport, the specific area of catalyst in the catalyst layers, the thickness of the membrane, the gas diffusion layer properties, the rate of methanol and water permeation and so on. Experimental investigating of the impact of these parameters one by one through is not time or cost efficient. In order to help understand the operation of a passive DMFC and locate the key parameters on cell performance, a theoretical model is essential.

5

In a previous work Oliveira et al. [18] report an intensive review on the work done in DMFC empirical and fundamental modelling. Despite the number of studies in DMFCs modelling only a few simulate passive DMFCs [6,19-23] and only a small part took into account thermal effects [6,19,22].

Since thermal management is a key issue in the portable DMFC system it is important to develop new models accounting for this effect and that can be a simple computer-aided tool to the design and optimization of passive direct methanol fuel cells.

Chen et al. [19] presented a one-dimensional model to describe a passive liquid-feed direct methanol fuel cell combining the effects of heat and mass transfer. The model provides the temperature profile along the different layers of a passive DMFC.

More recently, Chen et al. [22] presented a two-dimensional two-phase thermal model for passive direct methanol fuel cells (DMFC). The model was based on the unsaturated flow theory in porous media. The model is solved numerically using a home-written computer code to investigate the effects of various operating and geometric design parameters, including methanol concentration as well as the open ratio and channel and rib width of the current collectors, on cell performance.

As disadvantages, these two models [19, 22] consider the catalyst layers as an interface, so it is not possible to obtain the temperature and concentration profiles in these layers, and the authors assumed that the anode side is well insulated so no heat is lost from the anode side. This assumption may be very unrealistic in a passive DMFC working in a portable system.

Based on the model developed previously by the same authors [24], the goal of the present work is the development of a steady state, one-dimensional, multi-component and thermal model. The model takes into consideration the thermal and mass transfer effects, along with the electrochemical reactions occurring in the passive DMFC. The

6

model can be used to predict the methanol, oxygen, carbon dioxide and water concentration profiles in the anode, cathode and membrane as well as to estimate the methanol and water crossover and the temperature profile across the cell. The aim of the work is to produce a simplified model describing the main heat and mass transfer effects in a passive DMFC fuel cell and reproducing with satisfactory accuracy experimental data. The results of a simulation study using a developed model for passive DMFC´s are presented. The model was validated with data from experiments conducted in an in-house designed passive DMFC and with recent published data [3].

2. Model development

A schematic representation of a passive-feed direct methanol fuel cell is shown in Fig. 1, consisting of

- an acrylic plate (AAP) containing the fuel tank, a copper plate (ACP), a diffusion layer (AD) and a catalyst layer (AC) at the anode side;

- a polymer electrolyte membrane (M);

- a catalyst layer (CC), a diffusion layer (CD), a copper plate (CCP), and an acrylic plate (CAP) at the cathode side.

In a passive-feed DMFC the fuel, methanol or an aqueous methanol solution, and the oxidant are supplied to the reaction zone by natural convection. From the ACP through the AD and from the AC through the M, methanol solution is transported primarily by diffusion. In a similar way the transport of oxygen on the CCP, CD and CC is enhanced by diffusion. After the electrochemical reaction of methanol oxidation, witch takes place in the AC, the carbon dioxide produced moves counter-currently toward the AAP. At sufficiently high current densities carbon dioxide emerges in the form of gas bubbles

7

from the surface of the AC. In the CC, oxygen reacts with protons and electrons generating water. The water produced in CC moves counter-currently toward the CCP and also under some operating conditions, by back diffusion toward the anode.

The direct methanol fuel cell is complex system involving simultaneous mass, charge and energy transfer. In order to simplify the processes occurring in a DMFC the following simplifications and assumptions were made:

- the fuel cell is assumed to operate under steady-state conditions;

- the transport of heat and mass through the gas diffusion and catalyst layers is assumed to be a diffusion-predominated process and the convection effect is negligible;

- mass transport in the diffusion layers and membrane is described using effective Fick models;

- the thermal energy model is based on the differential thermal energy conservation equation (Fourier's law);

- pressure gradient across the layers is negligible;

- only the liquid phase is considered in the anode side, so carbon dioxide remains dissolved in solution;

- gaseous methanol and water are considered in the cathode;

- solutions are considered ideal and dilute;

- local equilibrium at interfaces is represented by partition functions;

- the catalyst layers are assumed to be a macro-homogeneous porous electrode so reactions in these layers are modelled as a homogeneous reaction;

- anode kinetics is described by step mechanism, with a rate expression similar to the used by Meyers et al. [25];

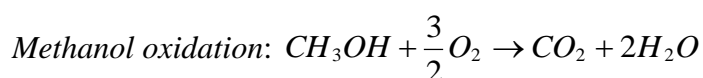- the anodic and cathodic overpotential is constant through the catalyst layers;
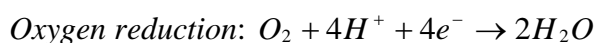
- cathode kinetics is described by Tafel equation;

- methanol and water transport through the membrane is assumed to be due to the combined effect of the concentration gradient between the anode and the cathode and the electro-osmosis force;

- on the anode side, the heat and mass transfer of methanol from the bulk solution to the ACP is assumed to be driven by natural convection;

- on the cathode side, the heat and mass transfer between the CCP and the ambient occur by natural convection;

- the heat generation by electrochemical reactions occurring in the catalyst layers is considered;

- when compared with the heat generated by electrochemical reactions and overpotential, the heat released by joule effects is ignored;

- the temperatures of the external walls of the cell (T_0 and T_9 in Fig. 1) are known;

- the heat flux generated in the catalyst layers is assumed to be constant.

2.1 Mass transport

Anode reaction:

Methanol oxidation: $CH_3OH + H_2O \rightarrow CO_2 + 6H^+ + 6e^-$

Cathode reaction:

Oxygen reduction: $O_2 + 4H^+ + 4e^- \rightarrow 2H_2O$

Methanol oxidation: $CH_3OH + \dfrac{3}{2}O_2 \rightarrow CO_2 + 2H_2O$

9

The transport process of methanol and water from the fuel tank to the ACP are described by

$$N_j = h_{mass,j}^{AAP}\left(C_j^0 - C_j^{AAP}\right) \tag{1}$$

where j represents methanol or water, N the molar flux, C the molar concentration and h_{mass} the mass transfer coefficient.

In the anode copper plate, diffusion and catalyst layer, the methanol and water flux are related to the concentration gradient by assuming Fickian diffusion [26] with an effective diffusivity $D_j^{eff,ACP}$ in the ACP, $D_j^{eff,AD}$ in the AD and $D_j^{eff,AC}$ in the AC. The methanol and water flux can be determined from:

$$N_j = -D_j^{eff,ACP}\frac{dC_j^{ACP}}{dx}, \ j \text{ represents methanol or water,} \tag{2}$$

$$N_j = -D_j^{eff,AD}\frac{dC_j^{AD}}{dx}, \ j \text{ represents methanol or water} \tag{3}$$

and

$$N_j = -D_j^{eff,AC}\frac{dC_j^{AC}}{dx}, \ j \text{ represents methanol or water} \tag{4}$$

The concentration at the AAP/ACP, ACP/AD and AD/AC interfaces is given by assuming local equilibrium with a partition coefficient K_2, K_3 and K_4, respectively. The boundary conditions for Eq. (2), (3) and (4) are (see Fig. 1)

$At\ x = x_2:\ \ C_{2,j}^{ACP} = K_2 C_j^{AAP},\ \ j$ represents methanol or water $\quad\quad (5)$

$At\ x = x_3:\ \ C_{3,j}^{AD} = K_3 C_{3,j}^{ACP},\ \ j$ represents methanol or water $\quad\quad (6)$

$At\ x = x_4:\ \ C_{4,j}^{AC} = K_4 C_{4,j}^{AD},\ \ j$ represents methanol or water $\quad\quad (7)$

$At\ x = x_5:\ \ C_j^{AC} = C_{5,j}^{AC},\ \ j$ represents methanol or water $\quad\quad (8)$

In fuel cells, all the fluxes can be related to a single characteristic flux, the current density or charge flux of the fuel cell. In the DMFC, the methanol flux is related to the current density and the permeation flux of methanol through the membrane, ($N_{CH_3OH}^{M}$), by:

$$N_{CH_3OH} = \frac{I_{Cell}}{6F} + N_{CH_3OH}^{M} \quad\quad (9)$$

where F represents the Faraday's constant and I_{cell} the cell current density.

At the anode side, the water flux is related to the current density and to the net water transport coefficient, α (defined as the ratio of the net water flux though the membrane from the anode to the cathode normalized by protonic flux), by:

$$N_{H_2O} = \frac{I_{Cell}}{6F}(\alpha + 1) \qu\quad (10)$$

The transport of methanol and water through the membrane is assumed to be due to the combined effect of the concentration gradient and the electro-osmosis force. The fluxes can be determined from:

11

$$N_{CH_3OH}^M = -D_{CH_3OH}^{eff,M} \frac{dC_{CH_3OH}^M}{dx} + \xi_{CH_3OH} \frac{I_{Cell}}{F} \tag{11}$$

$$N_{H_2O}^M = \alpha \frac{I_{Cell}}{6F} = -D_{H_2O}^{eff,M} \frac{dC_{H_2O}^M}{dx} + n_d \frac{I_{Cell}}{F} \tag{12}$$

The electro-osmotic drag (ξ_{CH_3OH}, n_d), in equations (11) and (12), is defined as the number of methanol or water molecules dragged by the hydrogen ions moving through the membrane.

The net water transport coefficient, α, can be calculated using the equation (12).

The concentration at the AC/membrane interface is given by assuming local equilibrium with a partition coefficient K_5. The boundary conditions for the integration of equations Eq. (11) and (12) is given by

$$At \ x = x_5: \quad C_{5,j}^M = K_5 C_{5,j}^{AC}, j \text{ represents methanol or water} \tag{13}$$

In the cathode catalyst layer, the methanol, water and oxygen flux are related to the concentration gradient by assuming Fickian diffusion [26] with an effective diffusivity $D_j^{eff,CC}$. The flux can be determined from:

$$N_j = -D_j^{eff,CC} \frac{dC_j^{CC}}{dx}, j \text{ represents methanol, water or oxygen} \tag{14}$$

It is here considered that the entire methanol crossing the membrane reacts at the cathode catalyst layer so the concentration at the CC/CD interface is zero. It is assumed that there is no oxygen crossover, so the oxygen concentration in CC/M interface is zero. The concentration of water and methanol at the membrane/CC interface and the concentration of water and oxygen at the CC/CD interface are given by assuming local

12

equilibrium with a partition coefficient K_6 and K_7, respectively. The boundary conditions for Eq. (14) are:

$$At \ x = x_6: \quad C_{6,j}^{CC} = K_6 C_{6,j}^{M}, \ j \ \text{represents methanol or water and} \ C_{6,O_2}^{CC} = 0 \tag{15}$$

$$At \ x = x_7: \quad C_{CH_3OH}^{CC} \cong 0, C_{H_2O}^{CC} = C_{7,H_2O}^{CC} \ \text{and} \ C_{O_2}^{CC} = C_{7,O_2}^{CC} \tag{16}$$

At the cathode catalyst layer, the oxygen reacts with the electrons and protons to produce water. However, part of oxygen fed is consumed due to methanol crossover to form an internal current and a mixed potential. Therefore the oxygen flux is related to the current density and the permeation flux of methanol through the membrane by:

$$N_{O_2} = \upsilon_{O_2} \frac{I_{Cell}}{4F} + \upsilon_{cross,O_2} N_{CH_3OH}^{M} \tag{17}$$

where

$$\upsilon_{O_2} = 1 \ \text{and} \ \upsilon_{cross,O_2} = \frac{3}{2}$$

The υ_{O_2} represents the stoichiometric coefficient of oxygen in the cathode reaction and the υ_{cross,O_2} stoichiometric coefficient of oxygen in the undesired cathode reaction.

At the cathode side, the water flux is related to the water production from the oxygen reduction reaction and methanol crossover oxidation and to the net water flux transported from the anode to the cathode by:

$$N_{H_2O} = \upsilon_{H_2O} \frac{I_{Cell}}{4F} + \upsilon_{cross,H_2O} N_{CH_3OH}^{M} + N_{H_2O}^{M} \tag{18}$$

13

where

$$\upsilon_{H_2O} = 2 \,, \ \upsilon_{cross,H_2O} = 2$$

The υ_{H_2O} represents the stoichiometric coefficient of water in the cathode reaction and the υ_{cross,H_2O} stoichiometric coefficient of water in the undesired cathode reaction.

In the cathode diffusion layer and cathode copper plate the oxygen and water flux are related to the concentration gradient by

$$N_i = -D_i^{eff,CD} \frac{dC_i^{CD}}{dx} \,, i \ \text{represents oxygen or water vapour} \tag{19}$$

$$N_i = -D_i^{eff,CCP} \frac{dC_i^{CCP}}{dx} \,, i \ \text{represents oxygen or water vapour} \tag{20}$$

where $D_i^{eff,CD}$ and $D_i^{eff,CCP}$ is the effective diffusion coefficient of oxygen and water in the CD and CCP.

The concentration at the CC/CD and CD/CCP interfaces is given by assuming local equilibrium with a partition coefficient K_7 and K_8. The boundary conditions for Eq. (19) and (20) are:

$$At \ x = x_7 : \quad C_{7,i}^{CD} = K_{7,i} C_{7,i}^{CC} \,, i \ \text{represents oxygen or water vapour} \tag{21}$$

$$At \ x = x_8 : \quad C_{8,i}^{CCP} = K_{8,i} C_{8,i}^{CD} \,, i \ \text{represents oxygen or water vapour} \tag{22}$$

Like at the anode side, the transport process of oxygen from the air to the CCP is described by:

$$N_i = h_{mass,i}^C \left(C_i^0 - C_{9,i}^{CCP} \right) \tag{23}$$

where i represents oxygen

We assume that the air at the CCP is in a saturated state, then the water vapour feed concentration (C_{8,H_2O}^0) is equal to water vapour concentration ($C_{8,H_2O}^{0,sat}$) and can be determined from the saturated pressure or moist air.

To account for the effect of methanol crossover on the cathode overpotential it is assumed that the methanol crossing the membrane completely reacts electrochemically at the cathode. In this way the internal current (I_{CH3OH}) due to methanol oxidation can be written as:

$$I_{CH3OH} = 6FN_{CH3OH}^M \tag{24}$$

where the methanol flux in the membrane (N_{CH3OH}^M) is obtained from Eq. (11).

The volumetric current density (j_A) expression for methanol oxidation is taken from Meyers et al. [25] as

$$j_A = aI_{0,ref}^{CH_3OH} \frac{kC_{CH_3OH}^{AC}}{C_{CH_3OH}^{AC} + \lambda \exp\left(\dfrac{\alpha_A \eta_A F}{RT_{AC}} \right)} \exp\left(\frac{\alpha_A \eta_A F}{RT_{AC}} \right) \tag{25}$$

15

where a represents the specific surface area of the anode, $I_{0,ref}^{CH_3OH}$ the exchange current density of methanol, α_A the anodic transfer coefficient, η_A the anode overpotential, T_{AC} anode catalyst layer temperature, k and λ are constants.

The current density is related to the volumetric current density using the following equation

$$I_{Cell} = \int_{x_5}^{x_6} j_A = \int_{x_5}^{x_6} a I_{0,ref}^{CH_3OH} \frac{k C_{CH_3OH}^{AC}}{C_{CH_3OH}^{AC} + \lambda \exp\left(\dfrac{\alpha_A \eta_A F}{RT_{AC}}\right)} \exp\left(\frac{\alpha_A \eta_A F}{RT_{AC}}\right) \tag{26}$$

Equation (26) is used to calculate the anode overpotential for a given I_{Cell}, assuming η_A as constant in the anode catalyst layer AC.

At the cathode, the electrochemical reaction is modelled using Tafel equation for the oxygen reduction taking in account the mixed potential. The cathode overpotential can then be determined from:

$$I_{Cell} + I_{CH_3OH} = I_{0,ref}^{O_2} \frac{C_{O_2}^{CC}}{C_{O_2,ref}^{CC}} \exp\left(\frac{\alpha_C \eta_C F}{RT_{CC}}\right) \tag{27}$$

where $I_{0,ref}^{O_2}$ reprsents the exchange current density of oxygen, α_C the cathodic transfer coefficient, η_C the cathode overpotential and T_{CC} cathode catalyst layer temperature.

The mass transfer coefficient in Eq. (1) and Eq. (23) can be determined from [27]:

$$Sh = \frac{h_{mass}L}{D} = \left[0.825 + \frac{0.387 \times Ra^{1/6}}{\left(1 + (0.492/Sc)^{9/16}\right)^{8/27}} \right]^2 \qquad (28)$$

where Ra is the Rayleigh number ($Ra = Gr \times Sc$), Sc the Schmidt number ($Sc = \nu/D$),

Gr is the Grashof number $\left(Gr = \dfrac{g\Delta CL^3}{C\nu^2} \right)$, L represents the length of the active area, D

the diffusion coefficient, g the gravitational acceleration and ν the kinematic viscosity.

2.2 Heat transport

Based on the simplifications and assumptions described previously the following

overall heat transfer equation can be proposed (see Fig. 1):

$$Q^{AC} + Q^{CC} = Q_1 + Q_2 \qquad (29)$$

The total heat generated in the DMFC is equal to the heat losses to the surrounding

environment at the anode and cathode.

Complementarly, the following heat transfer balances can be written:

$$Q_3 = Q^{AC} - Q_1 \qquad (30)$$

$$Q_2 = Q^{CC} + Q_3 \qquad (31)$$

At the anode, heat generated by the electrochemical reaction in the AC is given by

$$Q^{AC} = I_{Cell}\eta_A - I_{Cell}\left(\frac{\Delta H_A - \Delta G_A}{6F} \right) \qquad (32)$$

17

In this equation the first term represents the heat due to the activation and mass transfer overpotentials at the anode and the second term represents the entropy change of the anodic electrochemical reaction, with ΔH_A denoting the anodic reaction enthalpy and ΔG_A the Gibbs free energy.

In a similar way, the heat generated at the CC, can be determined from

$$Q^{CC} = (I_{Cell} + I_{CH_3OH})\eta_C - (I_{Cell} + I_{CH_3OH})\left(\frac{\Delta H_C - \Delta G_C}{4F}\right) - I_{CH_3OH}(\frac{\Delta H_A - \Delta G_A}{6F}) \qquad (33)$$

where the first term represents the heat due to the activation and mass transfer overpotentials and mixed potential caused by methanol crossover through the cathode and the second term represents the entropy change of the cathodic electrochemical reaction, with ΔH_C denoting the cathodic reaction enthalpy and ΔG_C, the Gibbs free energy and the third term denotes the entropy change of methanol oxidation reaction on the cathode due to methanol crossover.

In the anode acrylic plate section I and diffusion layer the heat flux Q_1 can be related to the temperature gradient across each layer, using the Fourier's law, as

$$Q = -K^l A_a \frac{dT}{dx} \qquad (34)$$

where l represents AAP$_{\text{sectionI}}$ or AD, K the thermal conductivity and A_a represents the active area.

In the anode acrylic plate section II the heat flux Q_1 can, also, be related to the temperature gradient across this layer, using Newton's law, as

18

$$Q = -h_{heat} A_a \Delta T \tag{35}$$

where h_{heat} represents the heat transfer coefficient.

At the cathode side and membrane, the heat fluxes Q_2 and Q_3 can be related to the temperature gradient across the CD and M layers as

$$Q = -K^t A_a \frac{dT}{dx} \tag{36}$$

where t represents CD or M.

In a passive DMFC the copper plate has holes machined on the surface, to allow the reactant to reach the catalyst layers (Figure 1). The establishment of the heat transport equations, in this layer, involved the consideration of two zones. In one zone the heat is transferred by conduction and in the other (holes) the heat is transferred by convection. Using the thermal resistance concept [27] we get:

$$Q = \frac{\Delta T}{R_{total}} \tag{37}$$

where

$$\frac{1}{R_{total}} = \frac{1}{R_{cond}} + \frac{1}{R_{conv}} \quad \text{since the resistances are in parallel} \tag{38}$$

$$R_{cond} = \frac{\delta}{A_1 \times K} \tag{39}$$

$$R_{conv} = \frac{1}{A_{holes} \times h_{heat}} \quad \text{and} \tag{40}$$

$$A_a = A_1 + A_{holes} \tag{41}$$

where R_{total} represents the total thermal resistance, R_{cond} the conduction resistance, R_{conv} the convection resistance, δ the thickness, A_{holes} total area of the holes and A_1 total area without the holes.

The differential equations describing the temperature profiles in the anode and cathode catalyst layers are:

$$\frac{d^2T}{dx^2} = \frac{Q^{AC}}{K^{AC}\delta^{AC}} \tag{42}$$

$$\frac{d^2T}{dx^2} = \frac{Q^{CC}}{K^{CC}\delta^{CC}} \tag{43}$$

where Q^{AC} and Q^{CC} are, respectively, the heat generated in the anode catalyst layer and cathode catalyst layer.

The boundary conditions for Eq. (42) and (43) are the temperatures at the walls (T_4, T_5, T_6 and T_7).

For these layers. Fourier's law gives

$$At \ x = x_4 : \quad Q_1 = -K^{AC}A_a\frac{dT}{dx} \tag{44}$$

$$At \ x = x_6 : \quad Q_3 = -K^{CC}A_a\frac{dT}{dx} \tag{45}$$

where $\dfrac{dT}{dx}$ is calculated using the temperature profile obtained from the integration of equations (42) and (43).

Finally, the heat transfer from the AAP section I and CCP to the ambient air can be described using the Newton's cooling law as

$$Q = -h_{heat}A_a\Delta T \tag{46}$$

The heat transfer coefficient, due to natural convection in Eq. (35), can be determined from [27]:

$$Nu = \frac{h_{heat}L}{K} = \left[0.825 + \frac{0.387 \times Ra^{1/6}}{\left(1 + (0.492/\text{Pr})^{9/16}\right)^{8/27}}\right]^2 \tag{47}$$

where Ra is the Rayleigh number ($Ra = Gr \times \text{Pr}$), Pr the Prandtl number ($\text{Pr} = \nu/K$) and Gr is the Grashof number $\left(Gr = \dfrac{g\beta\Delta T L^3}{\nu^2}\right)$.

2.3 Cell performance

The determination of methanol and oxygen concentrations at the catalyst layers, the temperature profiles and the anodic and cathodic overpotentials from the model equations enables prediction of the cell voltage, which can be expressed as:

$$V_{Cell} = E_{Cell} - \eta_A - \eta_C - I_{Cell}R_{Cell} \tag{48}$$

where

$$E_{Cell} = U_{O_2} - U_{CH_3OH} + \Delta T\left(\frac{\partial E}{\partial T}\right), \tag{49}$$

η_A and η_C are the anode and cathode overpotencials and the membrane resistance R_{Cell}

21

is given by

$$R_{Cell} = \frac{\delta^M}{\kappa}$$ (50)

where δ^M is membrane thickness and κ is the ionic conductivity of the membrane.

The results presented in the next section were obtained based on the parameters listed in Table 1.

3. Experiment

The experimental fuel cell consists of two acrylic end plates (open on the cathode side and with a reservoir on the anode side), two isolating plates, two gold plated copper connector plates (with 36 holes with a diameter of 6 mm to allow the reactants supply), two diffusion layers, two catalyst layers and a membrane. The membrane used was Nafion 115 the catalyst was Pt-Ru on the anode side with a loading of 4 mg/cm^2 and Pt-black on the cathode side with a loading of 4 mg/cm^2. The anode and cathode gas diffusion layers used carbon cloth from E-TEK, with a PTFE content of 30 wt.% (Fig 2).

In the experiments, a DMFC with an active area of a 25 cm^2 was used operating at atmospheric pressure by feeding aqueous methanol solution to the anode. The fuel cell temperature was controlled by a digital temperature controller and was set near ambient conditions, 20ºC. Five different methanol concentrations (1M to 5M) were tested in order to validate the model and analyse the effect of the methanol feed concentration on fuel cell performance.

The fuel cell test station was manufactured by Fideris Incorporated. The Methanol Test Kit (MTK) station comprises a methanol handling system, an oxidant gas handling

22

system and a linear electronic load [31]. The loadbank subsystem acts as a large variable power resistor which is capable of controlling the amount of impedance by selecting either how much current is passed through the loadbank, the voltage across the loadbank or power dissipated by the loadbank. The computer constantly monitors both current and voltage and these parameters are used to calculate and track the amount of power that the loadbank is dissipating at any one time.

4. Results and discussion

The developed model for the passive feed DMFC is rapidly implemented with simple numerical tools: Matlab and Excel.

In this section, examples of model predictions obtained after implementation of the model are presented. The conditions chosen to generate the simulations are similar to those used by the authors in their experiments. Since in passive DMFC systems the temperature rises with time due to the electrochemical reactions, in order to minimize this effect on the results presented in this section all the experiments were conducted at a controlled temperature, ensuring a constant temperature value during each experiment. In Figure 3 the predicted polarization curves for 1M to 5M methanol solutions, are presented. The open-circuit voltage is much lower than the thermodynamic equilibrium cell voltage as a result of methanol crossover. It can be seen that the fuel cell performance increases with an increase of the methanol feed concentration. Although for a 5M methanol concentration the performance decreases. This is due to the fact that higher methanol concentrations result in a higher methanol crossover. At the cathode side, methanol reacts with the oxygen to form a mixed potential. Hence, a higher methanol concentration leads to a higher mixed potential, thereby causing a lower cell performance. As we can see in Fig. 3 the present model describes well the experimental

results for all the range of current densities due to the integration, on the model, of the mass transfer effects at the cathode side. In Figure 4 data from Pan [3] was used to validate the model with results from other authors and already published. This work was chosen since the operating and design parameters used were similar to those reported in the present work. In Fig. 4 the predicted polarization curves for 1M and 3M methanol solutions, for a fuel cell temperature of 25ºC, are presented. According to this figure model predictions are close to experimental data presented by Pan [3]. The trends of the influence of the methanol concentration on fuel cell performance predicted in this paper are in accordance to the ones proposed by other authors [4,7-12,19,22].

Predicted methanol concentration profiles across de anode and membrane, are depicted in Figure 5, when the cell is feed with a 3M methanol solution at current densities of 10, 30 and 50 mA/cm^2. During the time considered for the analysis, the concentration profile at the methanol reservoir in the anode acrylic plate slightly decreases near the interface with the copper plate due to the fact that the diffusion of methanol occurs by natural convection (see Eq. (1)). In the other layers, the methanol concentration decreases due to mass transfer diffusion, methanol consumption in the catalyst layer and the methanol crossover through the membrane toward the cathode side. As can be seen by the plots of the concentration profile in the membrane presented in this figure the methanol crossover rate in the membrane decreases with the increase of current density.

Figure 6 shows the predictions of the methanol crossover as a function of current density for different methanol feed concentrations. As already referred the methanol that crosses the membrane reacts with oxygen on the cathode side forming a mixed potential and consequently a parasite current. This parasite current named leakage current represents fuel losses. According to Eq. (24) the methanol crossover can be expressed in terms of a leakage current witch gives a more understanding idea of the effect of the

loss in efficiency due to methanol crossover. As can be seen in Fig. 6, and as expected the leakage current increases with methanol concentration and decreases with current density. In this way, the leakage current and consequently the methanol crossover can be reduced by running the cell at low methanol concentrations and high current densities. The model predictions presented in this work concerning the methanol transport through the membrane are in accordance to previous work done by Abdelkareem et al. [7], Zhao et al. [12], Kho et al. [13] and Chen et al. [22].

Figure 7 show the water concentration across the anode and membrane. As is evident from this Figure, water diffusion occurs in ACP, AD, AC and M and water consumption in AC, so the water concentration profile decreases across these layers. The slope of the concentration profile in the membrane is higher than in the other layers showing a significant water crossover toward the cathode side.

Model predictions of the net water transport coefficient, α, are presented in Fig. 8 as a function of current density for different methanol feed concentrations. As can be seen from the plots, the methanol concentration has a large influence on the water crossover (α values). It should be noted that positive α corresponds to a net water flow from anode to cathode while negative α indicates that the net flow occurs in the opposite side. Figure 8 shows that for all the methanol concentration tested the values of α are positive, although low values of α are achieved using high methanol concentrations. This may be explained by the fact that lower methanol feed concentrations result in higher water concentrations on the anode side. The concentration gradient of water between the anode and cathode side is higher, so the transport of water towards the cathode is dominant. For higher methanol concentrations the amount of water present on the anode side is smaller and the water production in the cathode gives higher water concentrations at this side. In this situation, the water transport from the anode to the

cathode is still dominant (positive α) but, since the water concentration gradient is smaller less water is transported from the anode to the cathode side corresponding to smaller values of α.

In Figure 9, model predictions of α as a function of methanol feed concentration for different current densities are presented. It is evident that the methanol concentration has a large impact on the α values. Higher methanol concentrations result in low values of α. It is also evident that for higher values of the current density the impact of methanol concentration decreases. The effect of the methanol concentration on the net water transport coefficient was studied experimentally by Jewett et al. [5,17], Abdelkareem et al. [7], Zhao et al. [12], Song et al. [15] and Xu et al. [16]. The trends of the influence of the methanol concentration on the net water transport coefficient predicted by the model presented in this paper are in accordance to the ones proposed by these authors.

Figure 10 shows the oxygen concentration profiles across the cathode side, when the cell is fed with a 3M methanol solution at current densities of 10, 30 and 50 mA/cm^2. As can be seen from this Figure, the oxygen concentration decreases in CCP, CD and CC due to mass transfer diffusion. The slope of the concentration profile in the CC is higher than in the other layers due to oxygen consumption by the cathode reduction reaction, leading to an oxygen concentration of zero at the interface catalyst layer/membrane.

Figure 11 shows the temperature distribution in the active section of the cell (anode diffusion and catalyst layer, membrane and cathode catalyst and diffusion layer) for a methanol concentration of 3M and operating at different current densities. The data points represent the temperatures at the different layer interfaces. It can be seen in Fig. 11 that, for the three values of current density chosen, the temperature in the anode side

26

is higher than that in the cathode. This is because the heat generation rate by the anodic overpotential is higher than the endothermic heat demanded by the electrochemical reaction of methanol oxidation. With an increase in current density the difference between the anode and the cathode side increases as is evident in Fig. 11.

5. Conclusions

Based on the growing effort on the development of an efficient passive DMFC system and in order to help understand the operation of a passive DMFC and the key parameters on cell performance, a steady state, one-dimensional, multi-component and thermal model is presented, in this paper.

The model predicts the effect of the operating conditions (such as methanol concentration and fuel cell temperature) and the design parameters (the specific area of catalyst in the catalyst layers, the thickness of the membrane, the gas diffusion layer properties and thickness) on the fuel cell performance and power and on the water and methanol crossover. Due to their simplicity the model can be used to analyze the performance of a passive DMFC and to determine a single key (operating and design) parameter or combined parameters that would promote its efficiency most effectively. The model, also, predicts the methanol, oxygen and water concentration profile across the cell, as well as the temperature profile.

In this work, special attention is devoted to the effects of the methanol concentrations and the current density on the methanol and water crossover toward the cathode side. The model predicts the correct trends of the transport phenomena's in the passive DMFC and is in accordance with the experimental results and with published data [3].

As expected, high methanol concentrations achieve lower fuel cell performances due to the higher methanol crossover rates generated, however using lower methanol

27

concentrations significantly reduces the system energy density since more water is present on the anode side, will produce no power and will take up a large volume in the fuel reservoir. Thus, reducing the methanol transport from the anode to the cathode and the water content on the anode side is of significant importance to achieve higher cell performances and consequently increased power densities. With this easily to implement model, suitable operating and design conditions can be set-up for tailored MEAs in order to work at a high methanol concentration level without the sacrifice of performance. The present work is a starting point for more detailed experimental and modelling studies aiming the set-up of optimized and tailored MEAs adequate for DMFC portable applications.

References

[1] Q. Ye, T.S. Zhao, A natural-circulation fuel delivery system for direct methanol fuel cells, Journal of Power Sources, 147 (2005) 196-202.

[2] Y.H. Chan, T.S. Zhao, R. Chen, C. Xu, A self-regulated passive fuel-feed system for passive direct methanol fuel cells, Journal of Power Sources 176 (2008) 183–190.

[3] Y.H. Pan, Advanced air-breathing direct methanol fuel cells for portable applications, Journal of Power Sources 161 (2006) 282–289.

[4] J.G. Liu, T.S. Zhao, Z.X. Liang, R. Chen, Effect of membrane thickness on the performance and efficiency of passive direct methanol fuel cells, Journal of Power Sources 153 (2006) 61–67.

[5] G. Jewett, A. Faghri, B. Xiao, Optimization of water and air management systems for a passive direct methanol fuel cell, International Journal of Heat and Mass Transfer 52 (2009) 3564-3575.

[6] B. Xiao, A. Faghri, Transient modelling and analysis of a passive liquid-feed DMFC, International Journal of Heat and Mass Transfer 51 (2008) 3127-3143.

[7] M.A. Abdelkareem, N. Nakagawa, DMFC employing a porous plate for an efficient operation at high methanol concentrations, Journal of Power Sources 162 (2006) 114–123.

[8] R. Chen, T.S. Zhao, J.G. Liu, Effect of cell orientation on the performance of passive direct methanol fuel cells, Journal of Power Sources 157 (2006) 351–357.

[9] J. Liu, T.S. Zhao, R. Chen, C.W. Wong, Effect of methanol concentration on passive DMFC performance, Fuel Cells Bulletin (2005) 12–17.

[10] R. Chen, T.S. Zhao, Performance characterization of passive direct methanol fuel cells, Journal of Power Sources 167 (2007) 455–460.

[11] J.G. Liu, T.S. Zhao, R. Chen, C.W. Wong, The effect of methanol concentration on the performance of a passive DMFC, Electrochemistry Communications 7 (2005) 288–294.

[12] T.S. Zhao, R. Chen, W.W. Yang, C. Xu, Small direct methanol fuel cells with passive supply of reactants, Journal of Power Sources 191 (2009) 185–202.

29

[13] B.K. Kho, B. Bae, M.A. Scibioh, J. Lee, H.Y. Ha, On the consequences of methanol crossover in passive air-breathing direct methanol fuel cells, Journal of Power Sources, 142 (2005) 50-55.

[14] H. Kim, J. Oh, J. Kim, H. Chang, Membrane electrode assembly for passive direct methanol fuel cells, Journal of Power Sources, 162 (2006) 497-501.

[15] K. Song, H. Lee, H. Kim, MEA design for low water crossover in air-breathing DMFC, Electrochimica Acta, 53 (2007) 637-643.

[16] C. Xu, T.S. Zhao, In situ measurements of water crossover through the membrane for direct methanol fuel cells, Journal of Power Sources, 168 (2007) 143-153.

[17] G. Jewett, Z. Guo, A. Fagdri, Water and air management systems for a passive direct methanol fuel cell, Journal of Power Sources, 168 (2007) 434-446.

[18] V.B. Oliveira, D.S. Falcão, C.M. Rangel, A.M.F.R. Pinto, A comparative study of approaches to direct methanol fuel cells modelling, International Journal of Hydrogen Energy, 32 (2007) 415-424.

[19] R.Chen, T.S. Zhao, Mathematical modelling of a passive-feed DMFC with heat transfer effect, Journal of Power Sources, 152 (2005) 122-130.

[20] J. Rice, A. Faghri, A transient, multi-phase and multi-component model of a new passive DMFC, International Journal of Heat and Mass Transfer, 49 (2006) 4804-4820.

[21] V. Saarinen, O. Himanen, T. Kallio, G. Sundholm, K. Kontturi, A 3D model for the free-breathing direct methanol fuel cell: Methanol crossover aspects and validations with current distribution measurements, Journal of Power Sources, 172 (2007) 805-815.

30

[22] R.Chen, T.S. Zhao, W.W. Yang, C. Hu, Two-dimensional two-phase thermal model for passive direct methanol fuel cells, Journal of Power Sources, 175 (2008) 276-287.

[23] T.K. Yeh, C.H. Chen, Modeling and optimizing the performance of a passive direct methanol fuel cell, Journal of Power Sources, 175 (2008) 353-362.

[24] V.B. Oliveira, D.S. Falcão, C.M. Rangel and A.M.F.R. Pinto, Heat and mass transfer effects in a direct methanol fuel cell: A 1D model, International Journal of Hydrogen Energy, 33 (2008) 3818-3828.

[25] J.P. Meyers, J. Newman, Simulation of the Direct Methanol Fuel Cell-II. Modelling and Data Analysis of Transport and Kinetic Phenomena, Journal of Electrochemical Society, 149 (6) (2002) A718-A728.

[26] T.K. Sherwood, R.L. Pigford, C.R. Wilke, Mass Transfer, McGraw-Hill, 1975.

[27] Y.A. Çengel, Heat Transfer a Practical Approach, McGraw-Hill, 1998.

[28] B.L. García, V.A. Sethuraman, J.W. Weidner, R.E. White, Mathematical Model of a Direct Methanol Fuel Cell, Journal of Fuel Cell Science and Technology, Vol.1 November 2004 43-48.

[29] Thorsten Schultz, Experimental and Model-based Analysis of the Steady-state and Dynamic Operating Behaviour of the Direct Methanol Fuel Cell (DMFC), PhD thesis, 2004.

[30] R.C. Reid, J.M. Prausnitz, T.K. Sherwood, The Properties of Gases and Liquids, McGraw-Hill, 1977.

[31] V.B. Oliveira, D.S. Falcão, C.M. Rangel and A.M.F.R. Pinto, Modelling and experimental studies on a Direct Methanol Fuel Cell working under low methanol

crossover and high methanol concentrations, International Journal of Hydrogen

Energy, 34, 6443-6451

32

Caption for figures

Figure 1 - Schematic representation of a passive DMFC.

Figure 2 – «In-house» passive DMFC.

Figure 3 – Comparison of the model predictions of polarization curves for different methanol concentrations; dots: experimental data, lines: model predictions.

Figure 4 – Comparison of the model predictions of polarization curves for 1M and 3M methanol concentrations; dots: experimental published data [3], lines: model predictions

Figure 5 – Predicted methanol concentration profiles in the cell for different current densities. Operating conditions: methanol concentration 3M.

Figure 6 – Model prediction for methanol crossover for different methanol feed concentrations.

Figure 7 – Predicted water concentration distribution in the cell at different current densities. Operating conditions: methanol concentration 3M.

Figure 8 – Model predictions of the net water transport coefficient for different methanol concentrations.

Figure 9 – Influence of methanol concentration on the net water transport coefficient at different current densities.

33

Figure 10 – Predicted oxygen concentration profiles in the cell for different current densities. Operating conditions: methanol concentration 3M.

Figure 11 – Prediction for the temperature distribution in the cell at different current densities. Operating conditions: methanol concentration 3M.

34

Table 1

ACCEPTED MANUSCRIPT

<div align="center">**Table 1 –** Parameter values</div>

| Parameter	Value	Reference
U_{O_2}	1.24 V	[28]
U_{CH_3OH}	0.03 V	[28]
$\partial E / \partial T$	-1.4×10^{-4} V/K	[19]
κ	0.036 S/cm	[28]
δ^M	0.018 cm	[28]
$\delta^{AAPsectionI}, \delta^{AAPsectionII}$	0.50 cm	assumed
δ^{AD}, δ^{CD}	0.015 cm	assumed
δ^{AC}, δ^{CC}	0.0023 cm	assumed
$\varepsilon^{AD}, \varepsilon^{CD}$	0.71	assumed
ε^{AC}	0.81	assumed
ε^{CC}	0.86	assumed
a	1000 cm^{-1}	[28]
$I_{0,ref}^{CH_3OH}$	$9.425 \times 10^{-3} \exp((35570/R)(1/353-1/T))$ A/cm^2	[19]
$I_{0,ref}^{O_2}$	$4.222 \times 10^{-6} \exp((73200/R)(1/353-1/T))$ A/cm^2	[19]
k	7.5×10^{-4}	[28]
λ	2.8×10^{-9} mol/cm^3	[28]
α_A	0.52	[28]
α_C	1.55	[28]
K_{2-5}	0.8	assumed
K_{7-8,O_2}	1.25	assumed
K_6	0.001	assumed
K_{7-8,H_2O}	0.8	assumed
L	5 cm	assumed
$D_{O_2}^{eff,CD,CC}$	$\varepsilon^{CD,CC^{2.5}}\left[\left(T^{1.75} \times 5.8 \times 10^{-4}\right)/(27.772 \times P)\right]$ cm^2/s	[30]
$D_{O_2}^{eff,CCP}$	$\left[\left(T^{1.75} \times 5.8 \times 10^{-4}\right)/(27.772 \times P)\right]$ cm^2/s	[30]
$D_{CH_3OH}^{ACP}$	$\left[\left(7.608 \times 10^{-7} \times T\right)/(\mu_{H_2O} \times 9.485)\right]$ cm^2/s	[30]
$D_{CH_3OH}^{eff,AD,AC}$	$\varepsilon^{AD,AC^{2.5}}\left[\left(7.608 \times 10^{-7} \times T\right)/(\mu_{H_2O} \times 9.485)\right]$ cm^2/s	[30]
$D_{CH_3OH}^{eff,CC}$	$\varepsilon^{CC^{2.5}}\left[\left(T^{1.75} \times 5.8 \times 10^{-4}\right)/(33.904 \times P)\right]$ cm^2/s	[30]
$D_{CH_3OH}^{eff,M}$	$4.9 \times 10^{-6} \exp(2436 \times (1/333-1/T))$ cm^2/s	[28]
$D_{H_2O}^{ACP}$	$\left[\left(6.295 \times 10^{-7} \times T\right)/(\mu_{CH_3OH} \times 5.833)\right]$ cm^2/s	[30]
$D_{H_2O}^{eff,AD,AC}$	$\varepsilon^{AD,AC^{2.5}}\left[\left(6.295 \times 10^{-7} \times T\right)/(\mu_{CH_3OH} \times 5.833)\right]$ cm^2/s	[30]
$D_{H_2O}^{eff,CD,CC}$	$\varepsilon^{CD,CC^{2.5}}\left[\left(T^{1.75} \times 6.2 \times 10^{-4}\right)/(25.523 \times P)\right]$ cm^2/s	[30]
$D_{H_2O}^{eff,M}$	$2.0 \times 10^{-6} \exp(2060 \times (1/303-1/T))$ cm^2/s	[30]
ξ_{CH_3OH}	$2.5 \times x_{CH_3OH}$	[28]
n_d	$2.9 \exp(1029 \times (1/333-1/T))$	[19]
$\delta^{ACP}, \delta^{CCP}$	0.05 cm	assumed
K^M	0.0043 W/cmK	[29]
K^{AD}	$1.95 + 6,57 \times 10^{-4} T$ W/mK	[29]
K^{CD}	$1.71 + 2,96 \times 10^{-5} T$ W/mK	[29]
K^{AC}	$\left(1-\varepsilon^{AC}\right) \times 86,7 + \varepsilon^{AC}\left(0,341 + 9,26 \times 10^{-4}\right)$ W/mK	[29]
K^{CC}	$\left(1-\varepsilon^{CC}\right) \times 71 + \varepsilon^{CC}\left(0,0034 + 7,60 \times 10^{-5}\right)$ W/mK	[29]
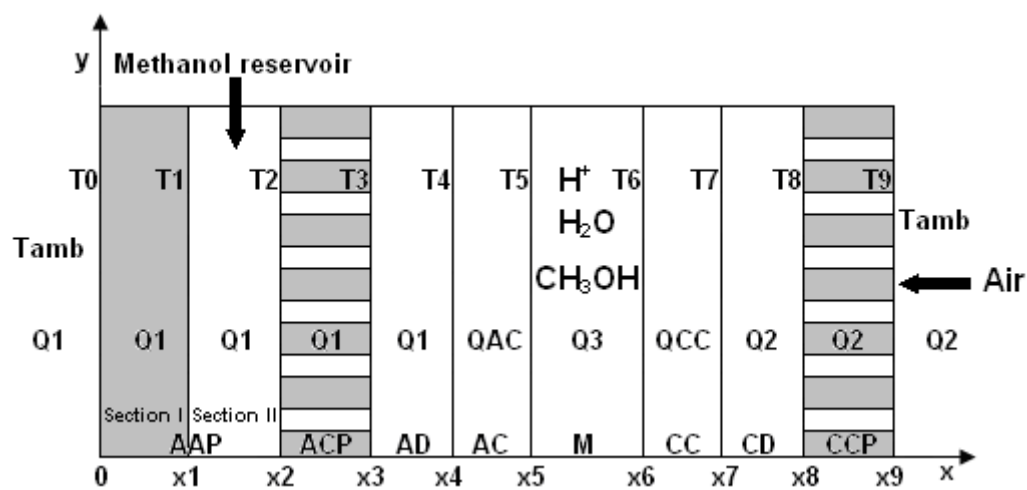
Figure 1

Oliveira *et al.* (2010)
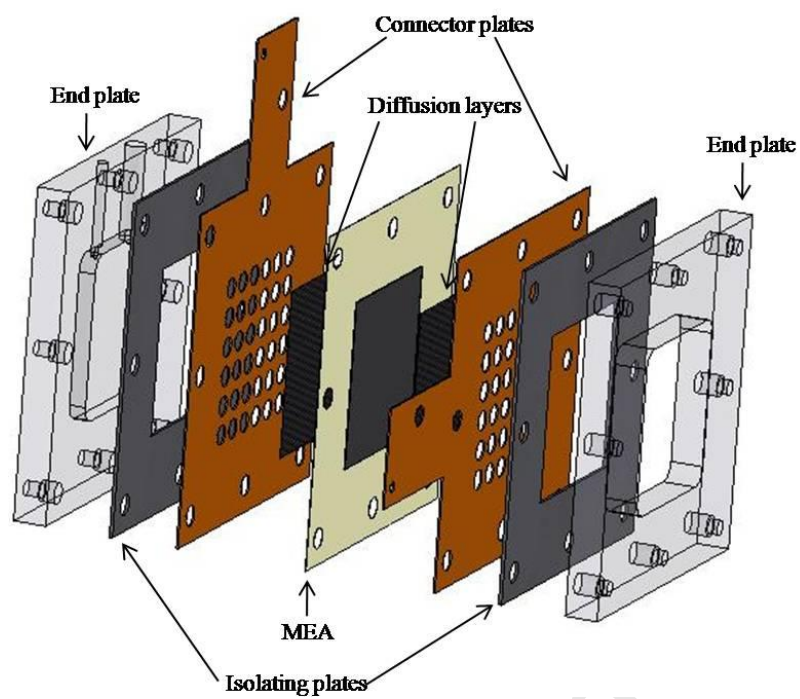
Figure 2

Oliveira *et al.* (2010)
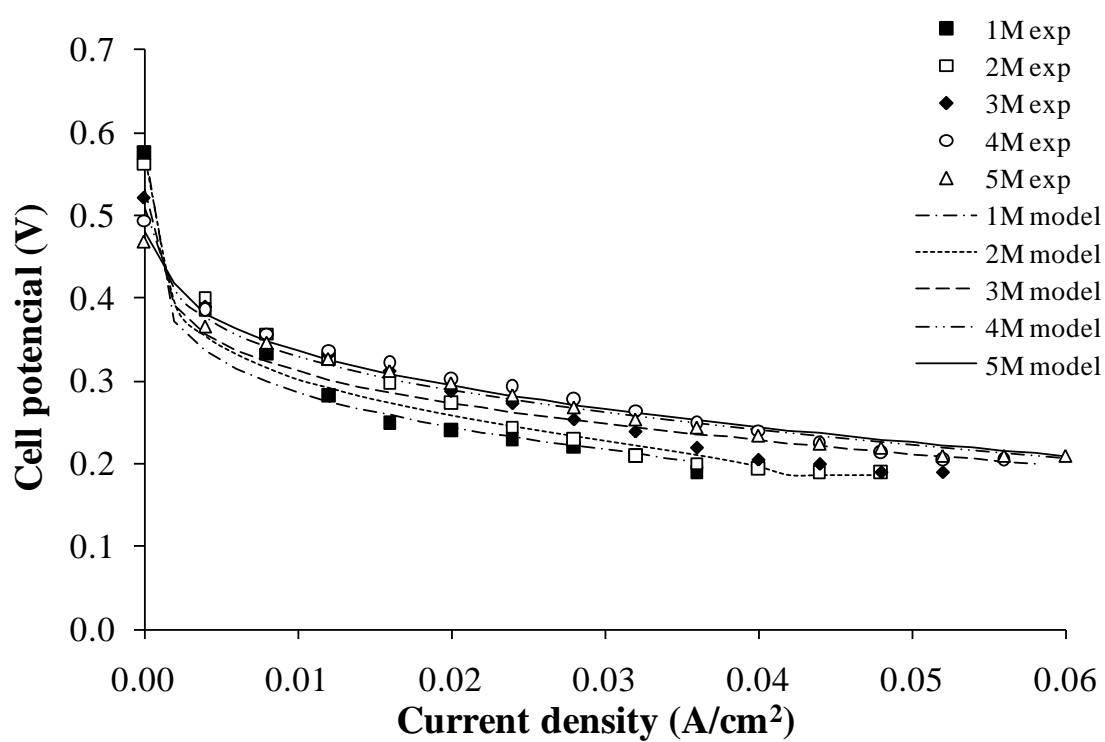
Figure 3

Oliveira *et al.* (2010)

Figure 4
[Click here to download Figure(s): Figure 4 new.doc](#)
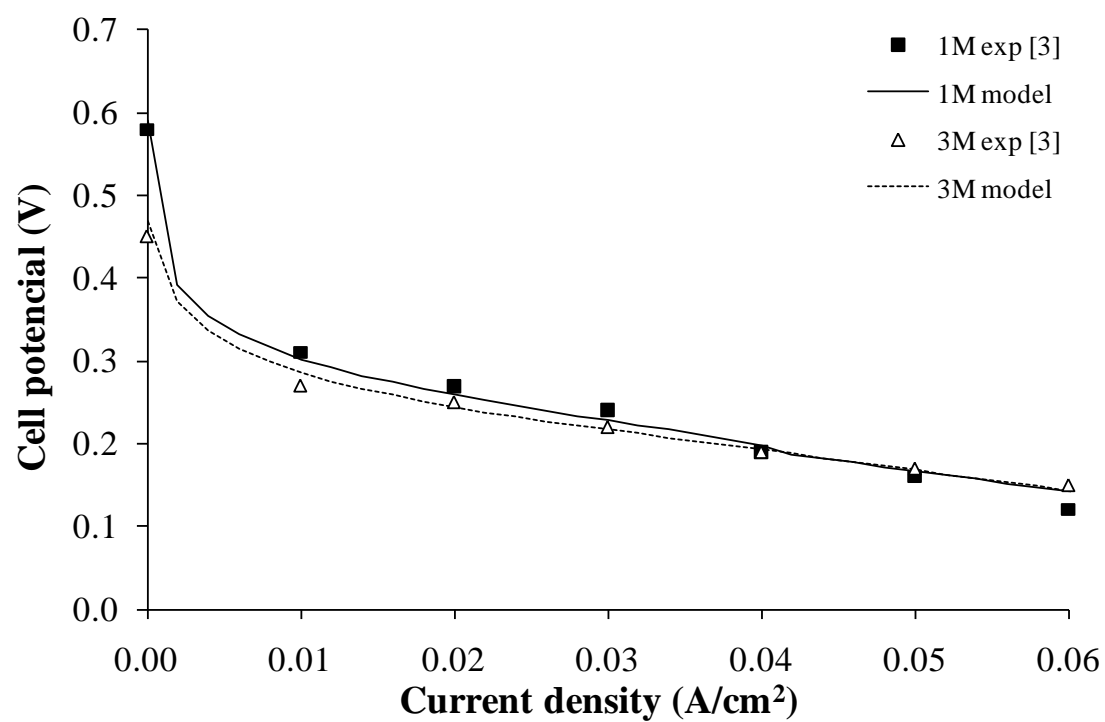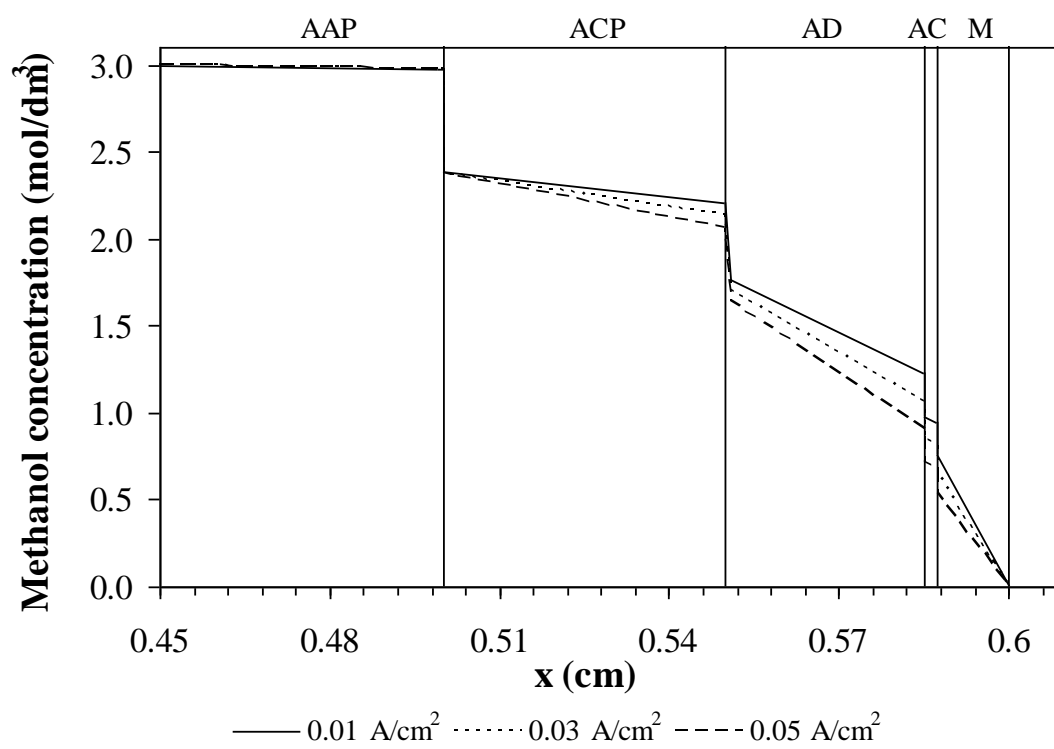
ACCEPTED MANUSCRIPT

Figure 4

Oliveira *et al.* (2010)
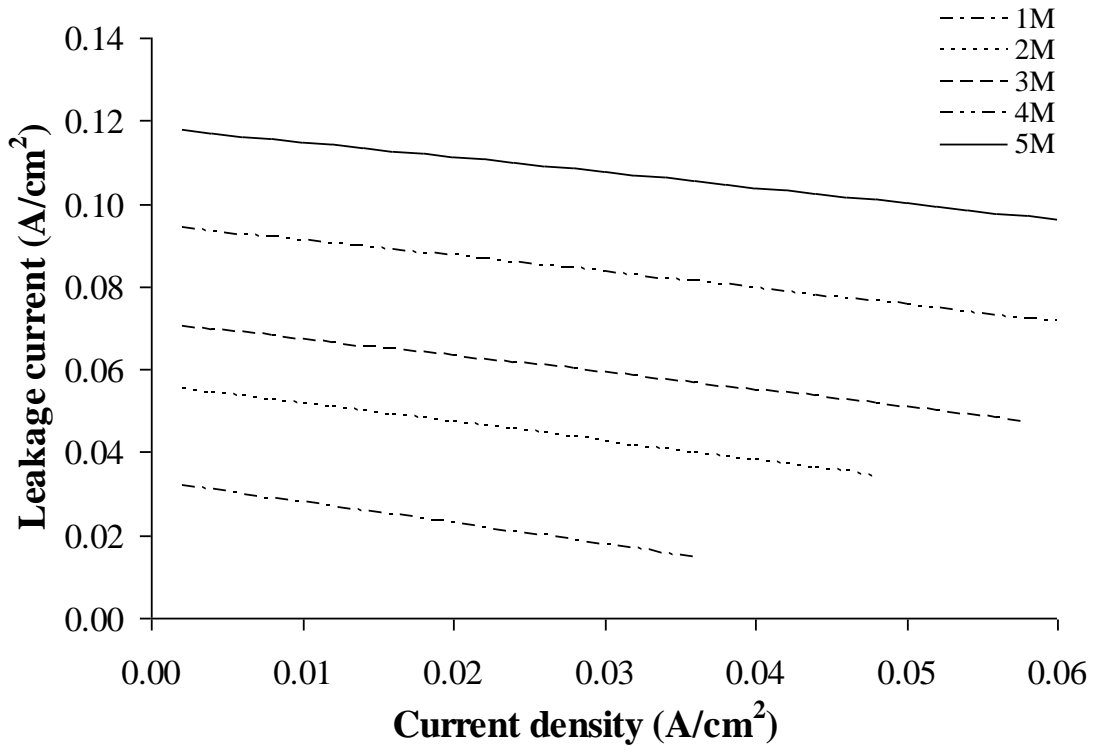
Figure 5

Oliveira *et al.* (2010)
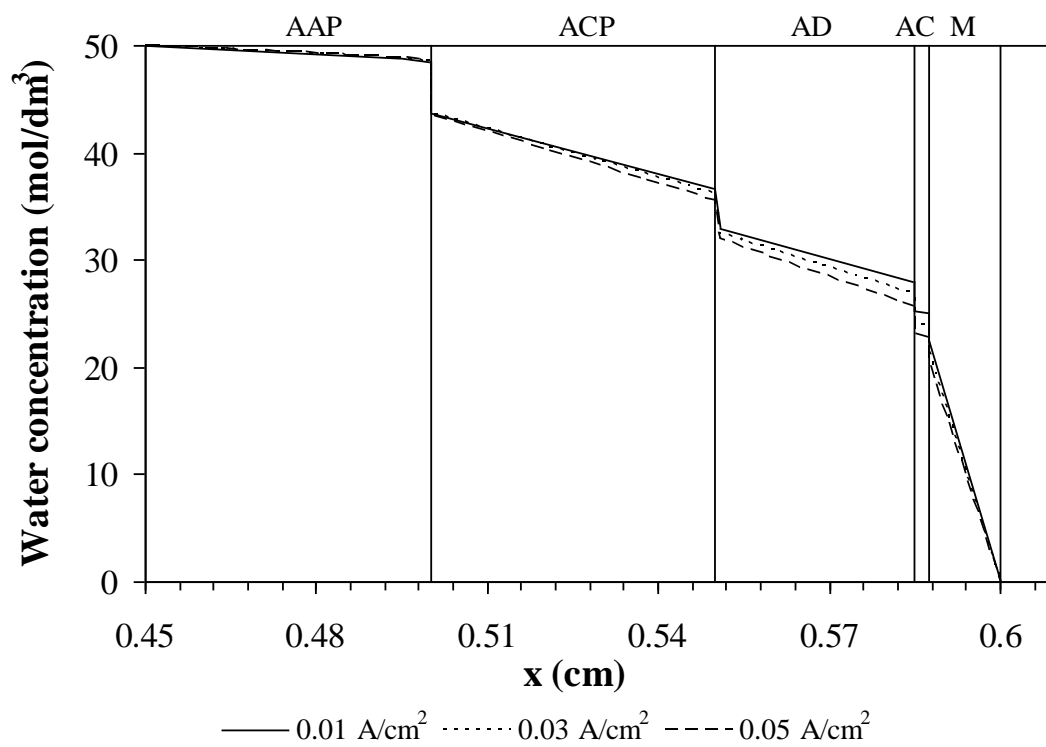
Figure 6

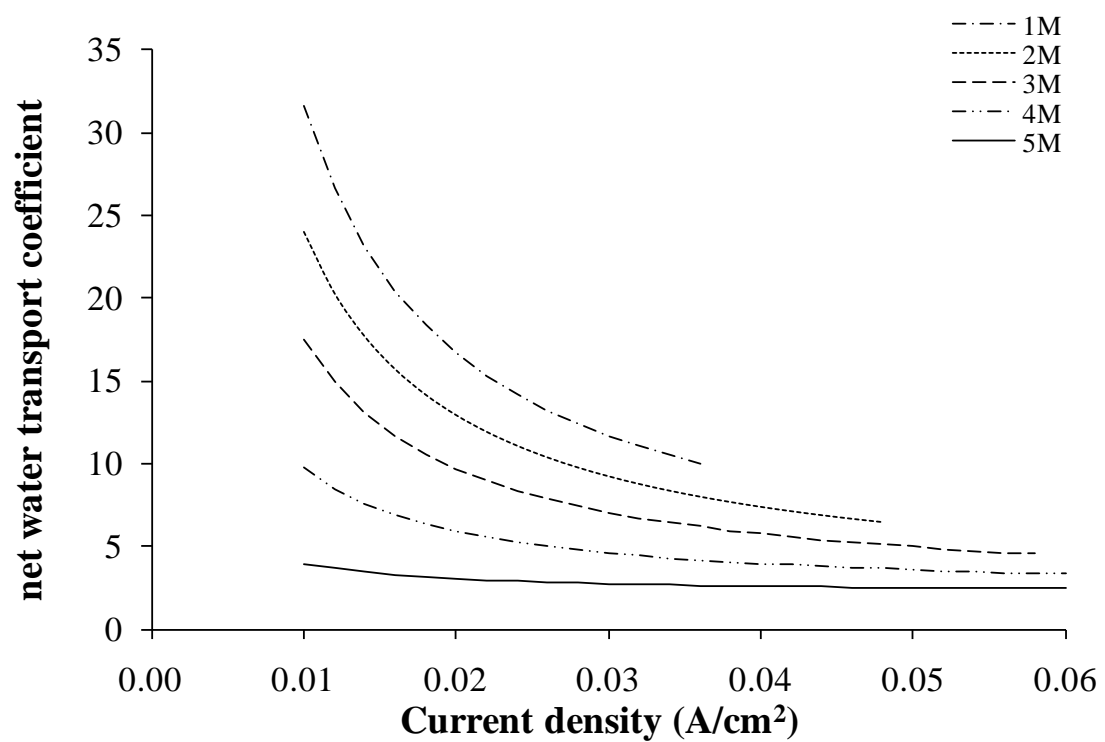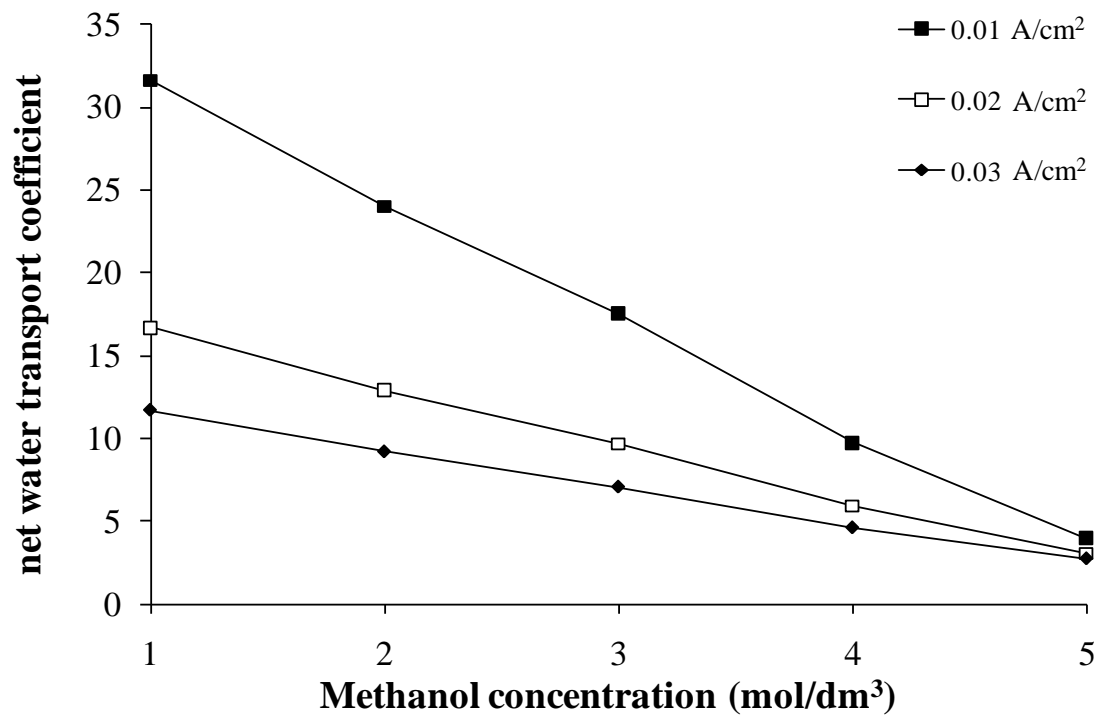Oliveira *et al.* (2010)

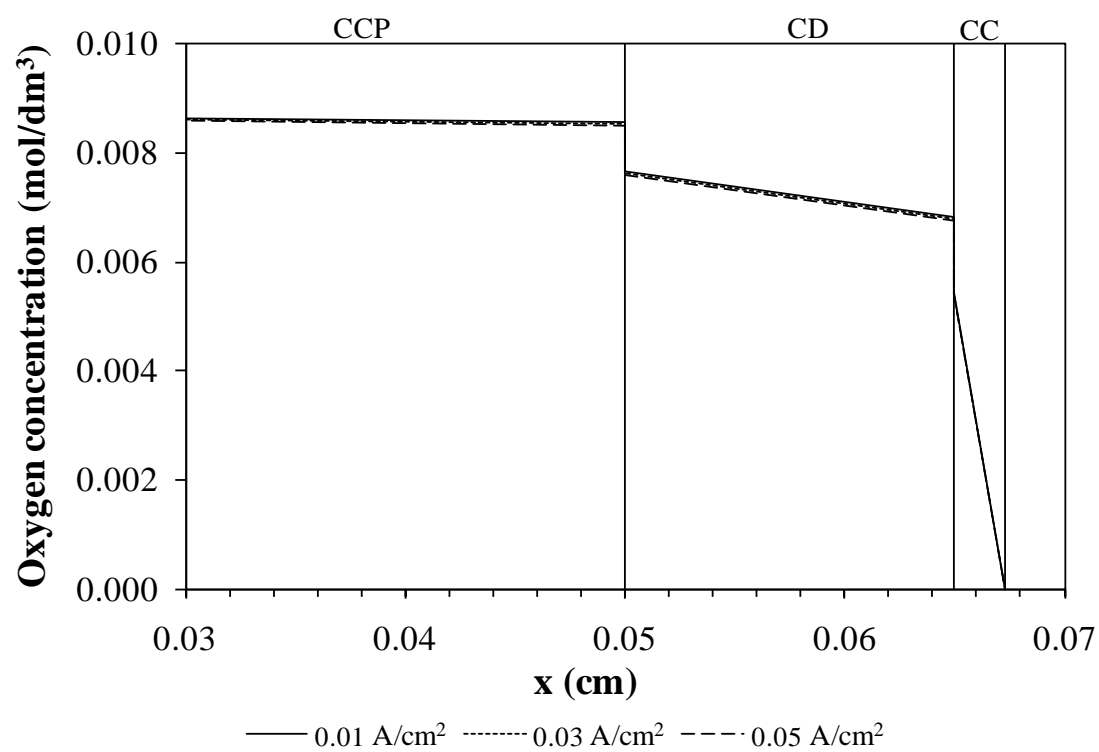Figure 7

Oliveira *et al.* (2009)
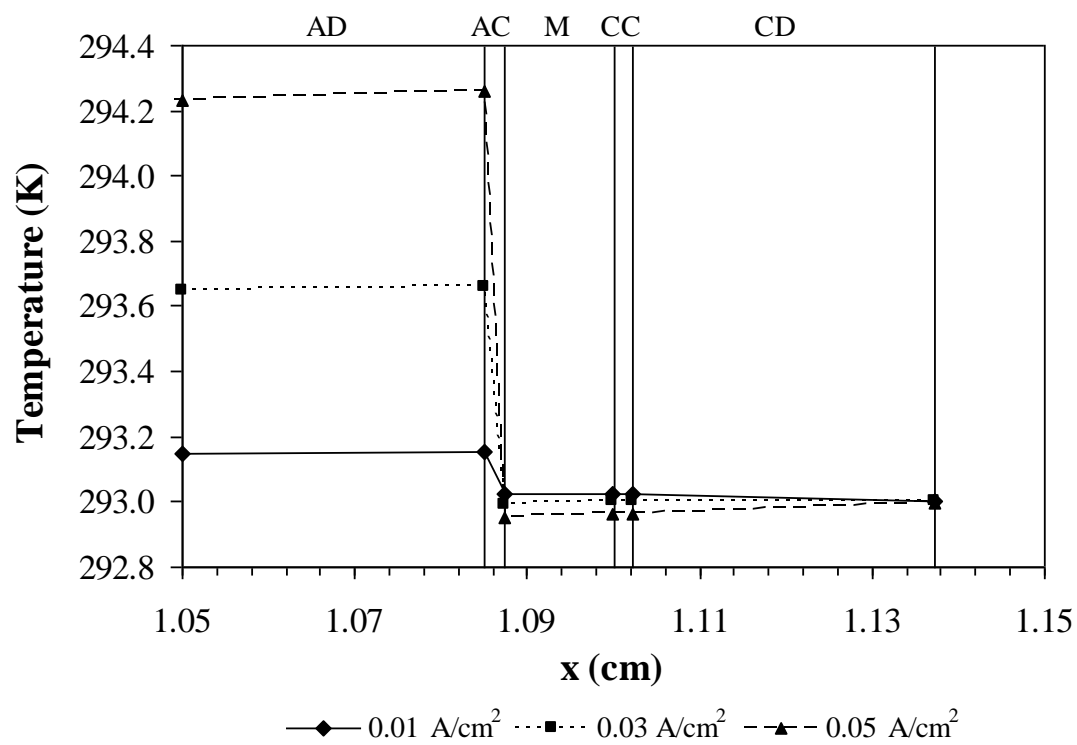
Figure 8

Oliveira *et al.* (2009)

Figure 9

Oliveira *et al.* (2009)

Figure 10

Oliveira *et al.* (2010)

Figure 11
Click here to download Figure(s): Figure 11.doc

ACCEPTED MANUSCRIPT

Figure 10

Oliveira *et al.* (2010)